

OVERVIEW OF RECENT RESULTS FROM HSX

D. T. ANDERSON, A. ABDU, A. F. ALMAGRI, F. S. B. ANDERSON, J. M. CANIK, W. GUTTENFELDER, C. LECHTE, K. M. LIKIN, H. LU, S. OH, P. H. PROBERT, J. RADDER, V. SAKAGUCHI, J. SCHMITT, J. N. TALMADGE,* and K. ZHAI *University of Wisconsin-Madison HSX Plasma Laboratory, 1415 Engineering Drive, Madison, Wisconsin 53706*

D. L. BROWER and C. DENG *University of California-Los Angeles, Electrical Engineering Department 66-127J Engineering IV Building, Los Angeles, California 90095-1594*

Received December 6, 2005

Accepted for Publication March 6, 2006

Recent results are summarized for the Helically Symmetric Experiment (HSX), which has the capability of running as a quasi-helically symmetric stellarator or as a more conventional, nonsymmetric stellarator. From X-ray measurements, we have demonstrated improved confinement of energetic particles. With central electron cyclotron heating, the density profiles in the quasi-symmetric configuration are peaked, in contrast to the hollow or flat profiles when the symmetry is broken. The difference in profiles is attributed to the lowering of the neoclassical thermodiffusive flux when the symmetry is present. The central electron temperature is ~ 200 eV higher for the quasi-symmetric configuration over the nonsymmetric case. The power deposition profiles are

similar for the two cases, implying that the neoclassical electron thermal conductivity is reduced with quasi-symmetry. Related to the good confinement characteristics in the quasi-symmetric mode of operation, fluctuations in the density and magnetic field, consistent with that of a global Alfvén eigenmode (GAE), are observed. While the neoclassical characteristics of the quasi-symmetric and nonsymmetric configurations are very different, we have yet to find, under present operating conditions, any significant difference (other than the possible GAE mode) in turbulence characteristics or blob formation at the plasma edge.

KEYWORDS: HSX, stellarator, quasi-symmetric

I. INTRODUCTION

Quasi-symmetric stellarators have the property that the Fourier spectrum of $|B|$ on a magnetic surface consists of a single dominant harmonic.¹ The Helically Symmetric Experiment² (HSX) is the first operational quasi-symmetric stellarator, with a helical direction of symmetry in the magnetic field strength. As a result of this symmetry, the neoclassical transport is reduced to the level of an axisymmetric device. The quasi-helically symmetric (QHS) magnetic field, with a toroidal mode number of $n = 4$ and poloidal mode number of $m = 1$, is produced with 48 nonplanar modular coils. In addition to the main modular coils, there is a set of auxiliary coils that are used to raise and lower the transform and the magnetic well depth as well as modify the magnetic field spectrum and the resulting neoclassical transport. Two configura-

tions in which the neoclassical transport is degraded with the addition of a toroidal mirror mode ($n = 4, m = 0$) are called the standard mirror (SM) and the phase shifted mirror (PSM). Thomson scattering measurements can be made close to the magnetic axis in PSM, while the axis is shifted ~ 1 cm inward for the SM configuration, making on-axis Thomson measurements impossible. The two configurations differ by the phase of the toroidal mirror term. For most of the results reported here, plasmas are produced and heated with 40 kW of second-harmonic electron cyclotron resonance heating (ECRH) at 28 GHz and a magnetic field strength of 0.5 T. Previously, we established that parallel viscous damping of flows is reduced with quasi-symmetry.³ In this paper we summarize recent experimental results obtained on HSX to further elucidate the differences between plasmas in quasi-symmetric versus nonsymmetric configurations. Some of the work presented here is still in progress and will be discussed in greater detail in upcoming papers.

*E-mail: talmadge@wisc.edu

II. CONFINEMENT OF ENERGETIC ELECTRONS

At an injected electron cyclotron heating (ECH) power up to 130 kW, the central temperature in the QHS configuration was in excess of 1 keV at a density of $1.5 \times 10^{12} \text{ cm}^{-3}$. Figure 1 shows the stored plasma energy measured by the diamagnetic loop, as well as the integrated Thomson density and temperature profiles, as a function of the line-averaged density for an injected power of 40 kW. It is seen that only at the higher plasma density does the integrated kinetic energy coincide with the diamagnetic loop measurements. At low density, the difference in the stored energy is due to a large population of nonthermal electrons, which are very well confined in the QHS configuration. This is also confirmed by the large nonthermal emission observed by electron cyclotron emission at low density.⁴

Better confinement of the nonthermal population in the QHS configuration is also demonstrated in Fig. 2, which shows the stored energy at a fixed density of $1.5 \times 10^{12} \text{ cm}^{-3}$ for the PSM configuration. This is plotted as a function of the ratio of the amp-turns in the auxiliary coils to the main coils (0% corresponds to the QHS configuration). As the configuration becomes more non-symmetric, the total stored energy from the diamagnetic loop approaches the stored energy from the integrated Thomson data. This indicates a reduction in the nonthermal contribution to the total energy.

A CdZnTe detector is used to detect the hard-X-ray flux for the QHS and SM configurations over a range of electron densities. Figure 3a shows that the integrated flux is higher for the QHS configuration, especially at the lower densities. Calculations of particle orbits and energies in a microwave field using a Lorentz model indicate that the more efficient heating in the quasi-symmetric configuration is due to the improved confinement. As seen in Fig. 3b, the integrated flux is higher for the QHS configuration at a fixed density of $4 \times 10^{11} \text{ cm}^{-3}$, while

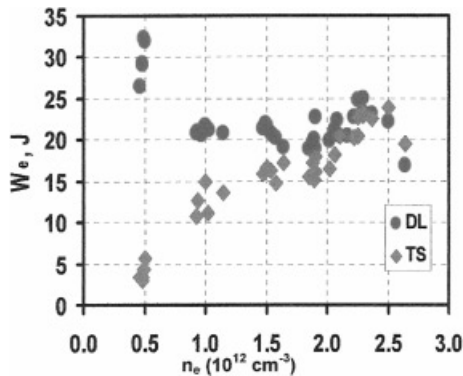


Fig. 1. Stored energy from a diamagnetic loop (circles) as well as from integrated Thomson profiles (diamonds) versus line-averaged density.

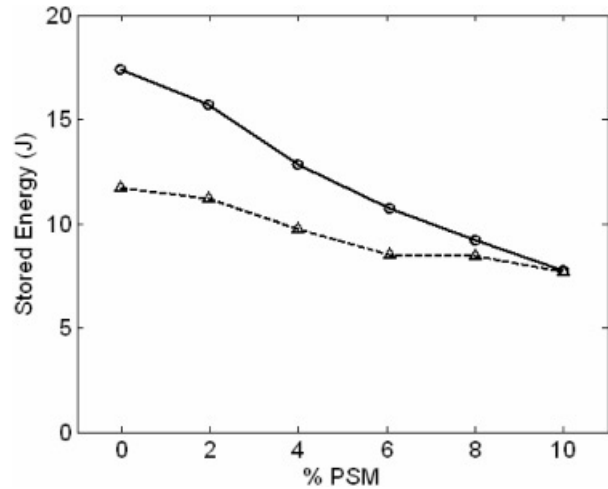


Fig. 2. Stored energy as function of asymmetry in the PSM configuration from the diamagnetic loop (circles) and integrated Thomson profiles (triangles).

the decay time for the signal in QHS (~ 7 ms) is longer than the Mirror configuration (~ 2.5 ms). This indicates that suprathermal electrons are confined for a longer time after the ECH heating source is turned off compared to the SM.

III. PARTICLE AND HEAT TRANSPORT

Density profiles in stellarators during ECH are typically flat or hollow. In Wendelstein 7-AS, for example, it has been shown that a peaked versus a flat density profile is a function of the balance between a thermodiffusive and an inward particle flux.⁵ In other machines such as IMS (Ref. 6), Heliotron-E (Ref. 7), and CHS (Ref. 8), the hollow profile was thought to be due to a convective flux driven by direct orbit losses. Calculations have shown that in large stellarators the thermodiffusive term may be so large as to drive hollow profiles that can cause serious density control problems.⁹ In particular, it may be necessary in a stellarator reactor to find a means by which to fuel the plasma core. We are interested in understanding how the density profile during ECH differs in quasi-symmetric versus nonsymmetric plasmas.

Thomson scattering is used to measure the electron temperature and density profiles. The system has ten spatial channels with 2-cm resolution along a 20-cm laser beam path. The particle source has been measured using a suite of absolutely calibrated H_α detectors with a poloidal array covering the plasma cross section at a fixed toroidal location, and several detectors distributed toroidally around the machine. The data from the H_α suite are interpreted based on neutral gas modeling with the DEGAS code.¹⁰

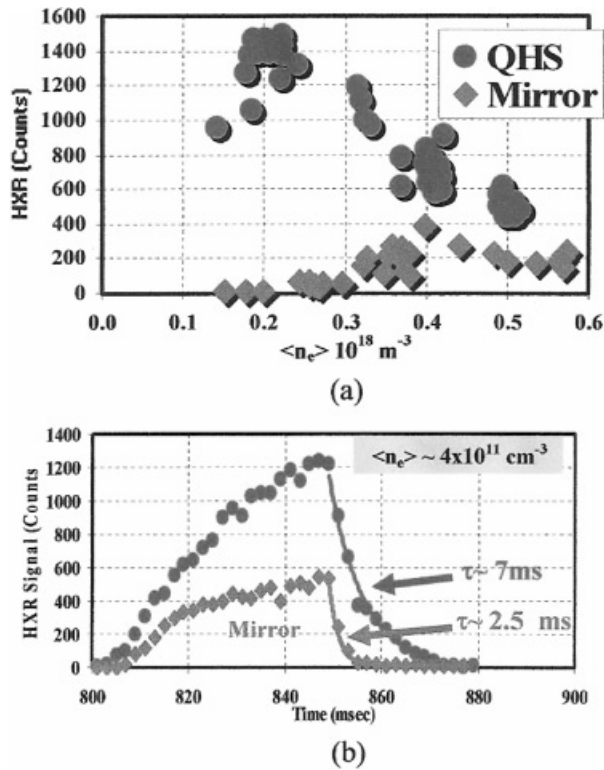


Fig. 3. (a) Hard-X-ray counts versus density for the QHS (circles) and SM (diamonds) configurations. (b) Hard X-rays versus time for the QHS and SM configurations.

Figure 4 shows a comparison of the electron density for the quasi-helical configuration to the PSM. In the PSM case, the axis is shifted downward allowing a Thomson data point on both sides of the axis. With central ECH resonance and peaked temperature profiles, the density profile is peaked for the QHS case. With the symmetry broken, the profile becomes flat to hollow in the Mirror configuration. The flatness of the profile for the PSM can be attributed to a larger thermodiffusive term. In contrast, neoclassical particle transport is much smaller for the QHS configuration, and the thermodiffusive term is too small to hollow out the profile.

The central temperature in the QHS case is $\sim 200 \text{ eV}$ higher than for the PSM configuration: 450 eV compared to 250 eV for similar absorbed power profiles. This is shown in Fig. 5. To study thermal transport, measurements of the absorbed power profile have been made using the Thomson scattering system. Measurements of the plasma density and temperature profiles were made in increments of $100 \mu\text{s}$ after the gyrotron turn-off for both the QHS and PSM configurations. In both cases the total absorbed power, based on the profile evolution, is 10 kW out of the 40 kW injected into the machine. The electron thermal diffusivity for the two configurations is $\sim 1 \text{ m}^2/\text{s}$ in QHS, compared to $\sim 3 \text{ m}^2/\text{s}$ for PSM. The

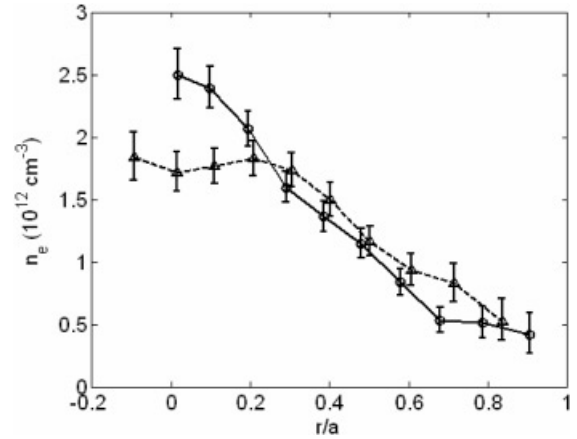


Fig. 4. Density profiles in the QHS (circles) and PSM (triangles) configurations.

total electron thermal conductivity is a sum of neoclassical and anomalous contributions. For the PSM case the experimental conductivity at the core is approximately the neoclassical value, while for the QHS configuration the neoclassical contribution is much lower than the experimental value. These results indicate that reducing the neoclassical thermal conductivity for the quasi-symmetric configuration increases the central electron temperature.

IV. FAST PARTICLE-DRIVEN INSTABILITY

Recent measurements on HSX have revealed the existence of coherent fluctuations in the electron density and magnetic field that suggest the presence of fast particle-driven instabilities. The mode has an $m = 1$

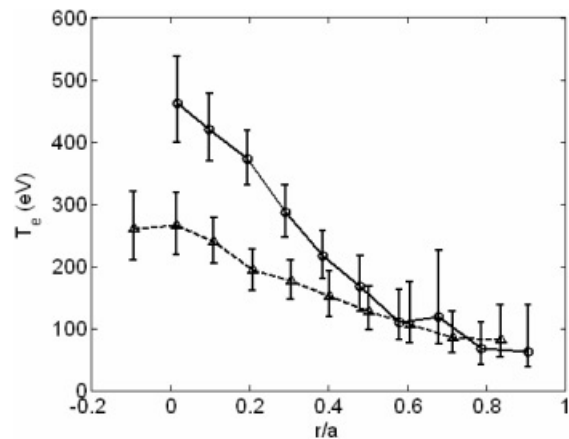


Fig. 5. Electron temperature profile for QHS (circles) and PSM (triangles) plasmas.

structure that peaks at $r/a \sim 0.5$. Figure 6 shows that the frequency of the mode decreases as the density increases, consistent with the dependence of a global Alfvén eigenmode (GAE):

$$\omega_{\text{GAE}} \leq k_{\parallel} v_A \frac{(m\ell - n)}{R} \frac{B}{\sqrt{4\pi n_i m_i}} \quad (1)$$

The mode has also been observed in deuterium and helium discharges and shows an Alfvénic scaling with ion mass density. Some initial theoretical work, in collaboration with Spong of Oak Ridge National Laboratory, further supports the possibility that this may be a GAE. Code runs from STELLGAP (Ref. 11), using the HSX quasi-helical equilibrium, predict a gap for the $m = 1$, $n = 1$ mode in the spectral region where the lower-frequency fluctuations are experimentally observed.

A distinguishing feature of these fluctuations is that they are predominantly observed in the QHS configuration and may be a result of the superior confinement of energetic particles. The instability quickly decreases with the introduction of a toroidal mirror term and is no longer observed when the percent ampere-turns in the auxiliary coils compared to the main coils is just 2%. The fast particle population is larger in the QHS configuration as compared to the Mirror configuration, as evidenced by the soft- and hard-X-ray signals.

V. EDGE TURBULENCE

Since advanced stellarators such as HSX have such low neoclassical transport, the role of anomalous transport becomes increasingly important. Turbulent structures were investigated for various magnetic configurations and plasma conditions using a number of Langmuir

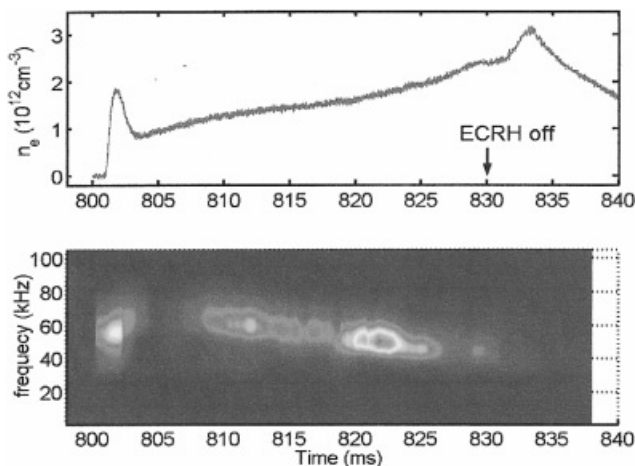


Fig. 6. Wavelet spectrum showing frequency decreasing (bottom) as density increases (top).

probe arrays. One array consists of a movable set of 16 pins aligned poloidally on a flux surface. A separate reference probe located in close toroidal proximity is positioned just inside the separatrix. By scanning the radial position of the 16-pin probe on a shot-by-shot basis, a two-dimensional, time-dependent correlation function can be created via cross correlation and conditional averaging techniques.¹² Additional four-pin probes are also located around the machine for measuring correlation lengths and times as well as turbulent-driven transport.

Figure 7 shows the two-dimensional correlation function of I_{sat} and V_{float} at multiple time lags measured in the QHS configuration. A turbulent structure with a radius of 1 to 1.25 cm, which is about ten times the drift radius ρ_s (the ion gyroradius evaluated at the electron temperature), is moving poloidally (upward) in the direction of the $E \times B$ drift during the course of 4 μs . No marked radial movement of the structures was observed. Each density structure is accompanied by a potential structure of the same sign. The phase between density and potential, i.e., the spatial displacement of the potential blob with respect to the density blob, usually is small. This is consistent with drift wave dynamics. At higher densities

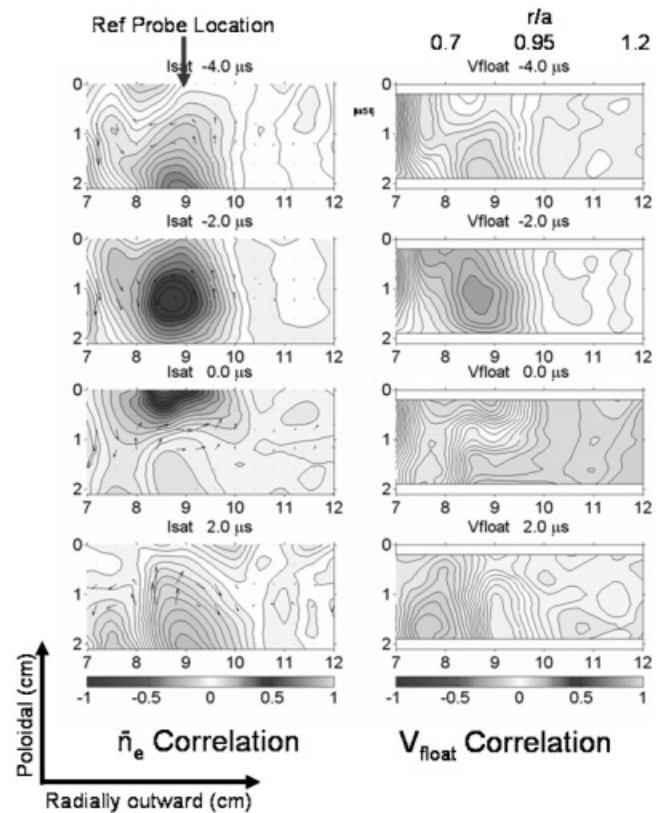


Fig. 7. Results of the cross correlation for a QHS discharge at a line-averaged density of 10^{12} cm^{-3} . A circular density structure (blob) moves poloidally upward, in the direction of the background $E \times B$ drift.

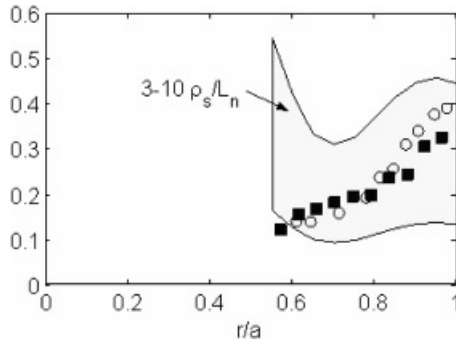


Fig. 8. Normalized I_{sat} fluctuation levels for QHS (circles) and SM (squares). Also shown is a range of mixing length estimates found in many experiments ($3-10 \rho_s/L_n$).

the $E \times B$ drift reverses, and the poloidal blob movement is also reversed. The blob characteristics did not vary much in the Mirror configuration as compared to QHS.

The fluctuation characteristics measured with the four-pin probes in various configurations obtainable in HSX are quite similar. Typical normalized fluctuation levels are 20 to 50% at the edge and within the range of mixing-length estimates $3-10\rho_s/L_n$, where L_n is the density scale length. This is shown by the normalized I_{sat} fluctuations in Fig. 8 for both the QHS and Mirror configurations at a line-averaged density of $1.0 \times 10^{12} \text{ cm}^{-3}$. Figure 9 shows that the calculated radial correlation lengths for the QHS and Mirror configurations at $r/a \approx 0.8$ are very similar. The correlation length decreases with increasing density, and since the local edge electron temperature also decreases with density, the inference is that the turbulence scale size is linked to ρ_s ($k_r \rho_s \sim k_\theta \rho_s \approx 0.1$). This is consistent with the gyro-Bohm nature of drift waves.

The turbulent-driven particle flux can be calculated via $\Gamma = \langle \tilde{n} \tilde{E}_\theta \rangle / B$, where density fluctuations are

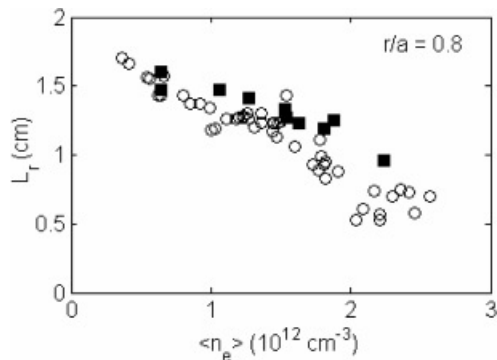


Fig. 9. Radial correlation lengths for QHS (circles) and SM (squares) discharges at $r/a \sim 0.8$ versus line-averaged density.

determined from the ion saturation current and poloidal electric field from two separate floating potential measurements. At line-averaged densities below $\sim 1.7 \times 10^{12} \text{ cm}^{-3}$, the measured turbulent particle flux is directed inward, as seen in Fig. 10. At higher densities, the turbulent particle flux is directed outward with magnitudes similar to those determined from H_α measurements and source rate modeling. The change in the direction of the turbulent particle flux has been observed in other stellarators, either in the presence of rational surfaces¹³ or with significant E_r shear¹⁴. The reason for this phenomenon in HSX is still under investigation.

VI. SUMMARY

A number of different physics issues have been explored in a quasi-symmetric stellarator and compared to configurations that have transport properties similar to those of conventional stellarators. Hard-X-ray fluxes are larger in the QHS mode of operation, as well as having longer decay times after the gyrotron turn-off. Density profiles are more peaked in the QHS configuration, probably due to the lower thermodiffusive flux. Hotter central electron temperatures are achieved as well, indicative of a reduction of the neoclassical electron thermal diffusivity in quasi-symmetric plasmas. We have found a coherent fluctuation in density and magnetic field that may be a result of the good confinement of energetic trapped particles in HSX. Finally, initial measurements of coherent structures and edge turbulence for QHS and Mirror plasmas indicate little difference in anomalous transport. This may help explain why the density and temperature profiles in the outer regions of the plasma are roughly the same. In the near future, the magnetic field and the available heating power will both be doubled so that further comparisons of quasi-symmetric and nonsymmetric plasmas can be made.

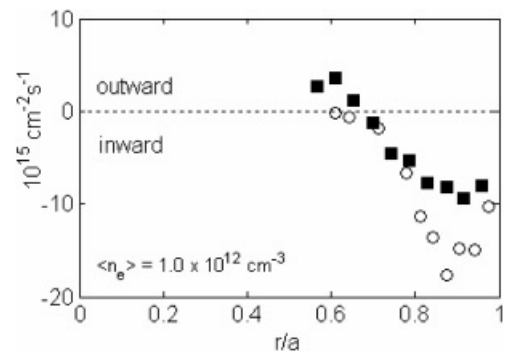


Fig. 10. Net measured turbulent particle transport in QHS (circles) and SM (squares) at $\langle n_e \rangle = 1.0 \times 10^{12} \text{ cm}^{-3}$.

REFERENCES

1. J. NUHRENBERG and R. ZILLE, *Phys. Rev. Lett.*, **114**, 129 (1986).
2. J. N. TALMADGE, V. SAKAGUCHI, F. S. B. ANDERSON, D. T. ANDERSON, and A. F. ALMAGRI, *Phys. Plasmas*, **8**, 5165 (2001).
3. S. P. GERHARDT, J. N. TALMADGE, J. M. CANIK, and D. T. ANDERSON, *Phys. Plasmas*, **12**, 056116 (2005).
4. K. M. LIKIN et al., "Electron Cyclotron Heating by X-Wave in the HSX Stellarator," *Proc. 13th Joint Workshop Electron Cyclotron Emission and Electron Cyclotron Heating*, Nizhny Novgorod, Russia, May 2004, p. 204 (2005).
5. U. STROTH et al., *Phys. Rev. Lett.*, **82**, 928 (1999).
6. J. N. TALMADGE et al., *Nucl. Fusion*, **29**, 1806 (1989).
7. H. ZUSHI, T. MIZUUCHI, K. NAGASIYAKI, T. NAKAYAMA, and B. J. PETERSON, *Plasma Phys. Control. Fusion*, **38**, 1307 (1996).
8. H. IDEI et al., *Fusion Eng. Des.*, **26**, 167 (1995).
9. H. MAASSBERG et al., *Plasma Phys. Control. Fusion*, **41**, 1135 (1999).
10. D. HEIFETZ et al., *J. Comput. Phys.*, **46**, 309 (1982).
11. D. A. SPONG, *Phys. Plasmas*, **10**, 3217 (2003).
12. C. LECHTE, S. NIEDNER, and U. STROTH, *New J. Phys.*, **4** (2002).
13. M. A. PEDROSA et al., *Plasma Phys. Control. Fusion*, **43**, 1573 (2001).
14. M. G. SHATS et al., *Phys. Rev. Lett.*, **84**, 6042 (2000).